

Symbiotic stars in X-rays

G. J. M. Luna,¹ J. L. Sokoloski,² K. Mukai,^{3,4} and T. Nelson⁵

¹ Instituto de Astronomía y Física del Espacio (IAFE), CC 67 - Suc. 28 (C1428ZAA) CABA – Argentina.
e-mail: gjmluna@iafe.uba.ar

² Columbia Astrophysics Lab 550 W120th St., 1027 Pupin Hall, MC 5247 Columbia University, New York, New York 10027 – USA

³ CRESST and X-ray Astrophysics Laboratory, NASA/GSFC, Greenbelt, MD 20771, USA

⁴ Department of Physics, University of Maryland, Baltimore County, 1000 Hilltop Circle, Baltimore, MD 21250, USA

⁵ School of Physics and Astronomy, University of Minnesota, 116 Church St SE, Minneapolis MN 55409 – USA.

ABSTRACT

Until recently, symbiotic binary systems in which a white dwarf accretes from a red giant were thought to be mainly a soft X-ray population. Here we describe the detection with the X-ray Telescope (XRT) on the *Swift* satellite of 10 white dwarf symbiotics that were not previously known to be X-ray sources and one that was previously detected as a supersoft X-ray source. The 10 new X-ray detections were the result of a survey of 41 symbiotic stars, and they increase the number of symbiotic stars known to be X-ray sources by 30%. *Swift*/XRT detected all of the new X-ray sources at energies greater than 2 keV. Their X-ray spectra are consistent with thermal emission and fall naturally into three distinct groups. The first group contains those sources with a single, highly absorbed hard component, which we identify as probably coming from an accretion-disk boundary layer. The second group is composed of those sources with a single, soft X-ray spectral component, which likely arises in a region where the winds from the two stars collide. The third group consists of those sources with both hard and soft X-ray spectral components. We also find that unlike in the optical, where rapid, stochastic brightness variations from the accretion disk are typically not seen, detectable UV flickering is a common property of symbiotic stars. Supporting our physical interpretation of the two X-ray spectral components, simultaneous *Swift* UV photometry shows that symbiotic stars with harder X-ray emission tend to have stronger UV flickering, which is usually associated with accretion through a disk. To place these new observations in the context of previous work on X-ray emission from symbiotic stars, we modified and extended the $\alpha/\beta/\gamma$ classification scheme for symbiotic-star X-ray spectra that was introduced by Müseret et al. based upon observations with the ROSAT satellite, to include a new δ classification for sources with hard X-ray emission from the innermost accretion region. Since we have identified the elusive accretion component in the emission from a sample of symbiotic stars, our results have implications for the understanding of wind-fed mass transfer in wide binaries, and the accretion rate in one class of candidate progenitors of type Ia supernovae.

Key words. (stars:) binaries: symbiotic – accretion, accretion disks; X-rays: binaries

1. Introduction

Symbiotic stars are wide binary systems in which a compact object, usually a white dwarf, accretes from a more evolved companion, a red giant. Recognizing that a red giant can transfer material onto different types of compact companions, we refer to those that we believe have white dwarf (WD) companions as *WD symbiotics* and those with neutron-star (or even black-hole) companions as *symbiotic X-ray binaries* (Masetti et al. 2006). Members of each of these groups do not necessarily display the optical spectroscopic features traditionally associated with symbiotic stars. In this paper, we primarily consider WD symbiotics. Due to the strong wind from the red giant, the binary system is surrounded by a dense nebula that is ionized by the UV radiation from the WD photosphere and/or the accretion disk. The orbital periods of symbiotic stars range from a few hundred to a few thousand days (Belczyński et al. 2000). Although in WD symbiotics the white dwarfs often have masses of approximately $0.6 M_{\odot}$ (Mikołajewska 2007), more massive white dwarfs — including those with masses close to the Chandrasekhar mass limit — are known to exist in WD symbiotic that experience recurrent nova outbursts or produce strong, hard X-ray emission (e.g. RS Oph, RT Cru; Sokoloski et al. 2006b; Luna & Sokoloski 2007).

WD symbiotics have been proposed as the progenitors of some type Ia supernovae (SNIa) either through the single or double degenerate channels. If the WD in WD symbiotics can accrete at a rate that is high enough for its mass to approach M_{Ch} , it could become a SNIa via the single-degenerate channel (e.g., Munari & Renzini 1992; Wang & Han 2010). Di Stefano (2010) proposed that some WD symbiotics might appear as “pre-double degenerate systems”, before the two WDs with a total mass of greater than M_{Ch} come close enough to merge within a Hubble time. There is observational evidence that at least some SNIa have a symbiotic system as a progenitor (Patat et al. 2007, Chiotellis et al. 2012, Dilday et al. 2012). To investigate the likelihood of WD symbiotics producing a significant fraction of SNIa, it is crucial to collect information needed to derive basic parameters such as M_{WD} and \dot{M} .

Unlike cataclysmic variables (CV), where accretion is driven by Roche-lobe overflow, the accretion mechanism in symbiotics is believed to be mainly some form of wind accretion (Bondi-Hoyle; Bondi & Hoyle 1944). Nevertheless, a consideration of angular momentum of the wind captured by the Bondi-Hoyle process leads to the conclusion that the formation of an accretion disk is common (Livio & Warner 1984). X-ray images of the WD symbiotic *o* Ceti show a stream of material flowing from the red giant towards the WD (Karovska et al. 2005), which can be understood in the context of the “wind Roche-lobe overflow”

scenario proposed by Podsiadlowski & Mohamed (2007). This model suggests that even if the red giant does not fill its Roche lobe, its wind can; and it is therefore focused toward the L1 point of the orbit, further increasing the likelihood of the formation of an accretion disk around the white dwarf. Sokoloski & Bildsten (2010), however, found no evidence that this mechanism is enhancing the accretion rate onto the white dwarf in this binary relative to the rate expected from pure Bondi-Hoyle wind-accretion.

If an accretion disk is present, the innermost region of the accretion disk, i.e., the boundary layer, can produce X-rays. As in dwarf novae, the boundary layer in the accretion disk of WD symbiotics can be a strong source of hard ($E \gtrsim 2$ keV) X-rays at accretion rates for which it is expected to be optically thin (e.g. $\dot{M} \leq 10^{-9.5} M_{\odot} \text{ yr}^{-1}$ for a $1 M_{\odot}$ WD; Narayan & Popham 1993). The temperature of the optically thin component, and hence the hardness of the X-ray spectrum, is a function of the gravitational potential well; the more massive the white dwarf the harder the spectrum. The combination of mass of the accreting object and accretion rate determines what the spectrum will look like in X-rays (Kylafis & Lamb 1982). White dwarfs accreting at a high rate can display a softer spectrum due probably to Compton cooling (e.g., RS Oph; Nelson et al. 2011) while a harder spectrum will be detected from an equally massive white dwarf that is accreting at a lower rate (e.g., T CrB, Luna et al. 2008).

If the white dwarf magnetic field is strong, greater than a few times 10^{5-6} G at the surface of the WD, hard X-rays are expected to arise from the magnetically channeled accretion flow onto a portion of the white dwarf surface. The observational signature of this type of accretion is the modulation of the light at the white dwarf spin period. In polars and intermediate polars (magnetic, accreting white dwarfs with low mass main sequence companions) the modulation is detected from optical to X-rays wavelengths (Warner 1995). In WD symbiotics, only one system has been detected with a coherent modulation of optical emission with a period of approximately 28 m (Z And; Sokoloski et al. 2006a) while an oscillation with a period of 1734 s was marginally detected (95% confidence) in X-rays from R Aqr (Nichols et al. 2007).

Soft ($E \lesssim 2$ keV) X-ray emission in WD symbiotics can also arise in several different circumstances. For example, soft X-rays could be produced if the system contains shocks with lower velocities than those of the shocks in a boundary layer or accretion column, as might be expected in a region where the winds from the white dwarf and red giant collide (Kenny & Taylor 2005). A hot accretion disk's corona, as proposed in LMXB (Ishida et al. 2009), or the red giant wind photoionized by hard X-rays would also be detected at soft X-ray energies.

Although a ROSAT-based classification scheme for the X-ray spectra of symbiotic stars (Muerset et al. 1997) provided a useful framework for early work on X-ray emission from these objects, the fact that multiple symbiotics are now known to produce X-rays with energies of greater than 20 keV indicates that a new treatment of X-rays from symbiotic stars is needed. Using pointed ROSAT observations, Muerset et al. (1997) detected 16 symbiotic stars and suggested a classification scheme based on the hardness of the spectra. They dubbed α -type those systems where emission with energies of less than $\lesssim 0.4$ keV originates in quasi-steady thermonuclear burning on the surface of the accreting white dwarf and β -type those with X-ray spectrum that peaks at energies of about 0.8 keV that might originate in a region where the winds from the two stars collide. Due to the small bandpass of ROSAT, the X-ray spectra of sources with harder emission than the β -types were only poorly characterized; they

were named γ types. This scenario changed dramatically with the discovery of very hard X-ray emission ($E > 50$ keV) from the symbiotic star RT Cru with *INTEGRAL* (Chernyakova et al. 2005) and *Swift* (Tueller et al. 2005) in 2005. Since then, three more systems were observed to have X-ray emission with energies higher than ≈ 10 keV (T CrB, SS73 17, CH Cyg; Smith et al. 2008, Kennea et al. 2009, Mukai et al. 2007). The observed spectra are all compatible with highly absorbed ($n_H \approx 10^{22-23} \text{ cm}^{-2}$) optically thin thermal emission with plasma temperatures corresponding to $kT \approx 5-50$ keV. Given that modulation has not been detected in their light curves, the hard X-ray emission most likely originates in the accretion disk's boundary layer. The X-ray spectral fitting indicated that, like the WD symbiotics that produce softer X-rays, these hard X-ray producing symbiotics contain white-dwarf accretors. The high, variable absorption may explain why these systems were not detected in all sky surveys such as RASS. In the neutron-star accretors (i.e., symbiotic X-ray binaries), the broad-band X-ray spectra are usually due to optically thick Comptonizing plasma with no emission lines (see e.g., Marcu et al. (2011) and references therein).

In this article, we present the results of a *Swift* fill-in program whose aim was to search for hard X-ray emission from WD symbiotic, and a Target of Opportunity (ToO) program to identify the X-ray counterpart of IGR J17197-3010. We describe *Swift* observations of 10 newly discovered hard X-ray emitting WD symbiotics and one previously known supersoft source. With these new, broad-band X-ray data, it becomes necessary to introduce a classification scheme that is a modification and extension of the one proposed by Muerset et al. (1997). Observations and data analysis details are presented in Section 2 while results are shown in Sections 3 and 4. Section 5 presents the discussion and concluding remarks.

2. Observations and data reduction.

During cycle 6, *Swift* observed 41 symbiotics using the X-ray Telescope (XRT) and the Ultraviolet/Optical Telescope (UVOT). We obtained these observations as part of a *Swift* Fill-in (6090813, PI: J. Sokoloski) and a Target of Opportunity (ToO) program (Target ID 31648, PI: G. J. M. Luna). Except for SWIFT J171951.7-300206, which we found serendipitously in the field of IGR J17197-3010 (Luna et al. 2012), we selected our targets from the symbiotic-star catalog of Belczyński et al. (2000), which lists 188 confirmed and 30 suspected symbiotics. After excluding objects with previous X-ray detections (except for StH α 32, which we retained by accident), we chose the sources that are the most likely to be nearby and therefore the most likely to be detectable with *Swift*. The majority of objects in the Belczyński et al. catalog do not have distance estimates available in the literature, so we used source brightness in the V and K bands (which are dominated by light from the red giant) as a proxy for proximity, including all objects with either V brighter than 10.9 mag (but fainter than the UVOT optical brightness limit) or K brighter than 5.0 mag. Since symbiotic stars are a disk population, objects with very large $|b|$ are also preferentially nearby. Our target list thus also included all objects with $|b| > 11^{\circ}$. *Swift* observed all objects for approximately 10 ks (in most cases using multiple visits) in Photon Counting mode (PC) of the XRT. The UVOT observations used either the UUU ($\lambda 3465 \text{ \AA}$, FWHM=785 \AA), UVW1 ($\lambda 2600 \text{ \AA}$, FWHM=693 \AA), UVM2 ($\lambda 2246 \text{ \AA}$, FWHM=498 \AA) and/or UVW2 ($\lambda 1938 \text{ \AA}$, FWHM=657 \AA) filters (Poole et al. 2008). The observation log is detailed in Table 1. In total, *Swift* devoted 433.6 ks to this project.

We used the XIMAGE package to search for X-ray emission from each target, with a S/N threshold for detection of 3σ (on average 0.0016 c s^{-1}). All sources, except Y Cra, were detected at their catalogue positions, which were inside the *Swift*/XRT error circles (about 3 arcsec in radius). We extracted source X-ray spectra, event arrival times and light curves from a circular region with a radius of 20 pixels ($\approx 47''$) whose centroid we determined using the tool `xrtcentroid`. To correct for the presence of dead columns on the XRT CCDs during timing analysis of XRT data, we used the standard tool `xrtlccorr`. We extracted background events from an annular region with inner and outer radii of 25 and 40 pixels, respectively. We built the ancillary matrix (ARF) using the tool `xrtmkarf` and used the `swxpc0to12s0.20070901v011.rmf` response matrix provided by the *Swift* calibration team. We searched for modulations in the X-ray light curves by calculating the Z_1^2 statistic (Buccheri et al. 1983) from source event arrival times in the frequency range $f_{\min}=1/T_{\text{span}}$ to $f_{\max}=1/(2t_{\text{frame}})$ with a step $\Delta f=A/T_{\text{span}}$, where T_{span} is the difference between the last and first event arrival time, t_{frame} is the readout time (2.5073 s for the *Swift*/XRT/PC), and $A=50$ is the oversampling factor.

During each visit, *Swift* also obtained UVOT exposures. From the pipeline-reduced data, using the `uvotmaghist` script, we extracted the source count rate for each exposure from a circular region of $5''$ radius and background from an annular region of $10''$ and $20''$ inner and outer radii respectively. For those objects that were not detected in individual exposures, we added the exposures using the `uvotimsum` tool to improve the detection efficiency and extracted the count rate or its upper limit using the `uvotsource` tool. No period search was performed on the UVOT data due to the small number and scarcity of the exposures on each object. We quantified the stochastic variability in the UVOT light curves by comparing the expected standard deviation from Poisson statistics only (s_{exp}) with the measured standard deviation (s) during each visit.

3. Survey results.

Our survey detected X-ray emission from 11 sources, with spectra spanning the range of known X-ray characteristics observed in WD symbiotics. In the ultraviolet, unlike at optical wavelengths, we detect strong flickering in most of the sources in our sample.

3.1. X-ray data

The XRT detected 11 out of 41 targets in our survey, and all of the detected sources had X-ray spectra consistent with thermal emission. From the 11 detections, one source was confirmed as a supersoft source while the remaining 10 were detected up to energies greater than 2.4 keV, with 0.3-10.0 keV count rates ranging from 0.0017 to 0.026 counts s^{-1} . The spectra hint at the presence of unresolved emission lines in the ~ 1 -2 keV (e.g. S XV, S XVI, Si XIII, Si XIV, Mg XII, Mg XI) and ~ 6.4 keV regions (e.g. Fe K α , Fe XXV, Fe XXVI) consistent with the presence of optically thin thermal emission. The hardness ratios of the WD symbiotics with detectable emission above 2.4 keV ranged from $r = 0.14$ to 9.85 (where we define r as the ratio of count rates at 2.4-10.0 keV and 0.3-2.4 keV energy ranges). The X-ray spectra (Figure 1 and 2) are consistent with optically thin thermal emission for all of the X-ray sources other than StH α 32 2), with 5 sources showing two distinct spectral components (NQ Gem, ZZ CMi, V347 Nor, BI Cru and UV Aur) and 5 showing a single dominant spectral component (Hen 3-461, CD-28 3719, ER Del,

Y Cra and SWIFT J171951.7-300206). We did not detect modulation in the X-ray light curves in any source of our sample. The observations were sensitive to pulsed fractions of 44% (for NQ Gem, from which we detected the largest number of photons) or more. Because of the low number of counts, we used the C statistic (Cash 1979) throughout the spectral fitting procedure of the unbinned data. To determine whether the model fit appropriately described the data, we calculated the goodness-of-fit as implemented in Xspec (Arnaud 1996), which simulates spectra many times based on the model and returns the number of simulations that have a fit statistic lower than that of the data. Ideally, if approximately 50% of the simulations have a fit statistic lower than that from the data, then the data are well-reproduced by the model. However, some issues have been reported when fitting models with less than 100 counts in total (Arnaud et al. 2011). For those objects that we detected with less than ≈ 100 counts, we use visual inspection of the fit residuals to distinguish between two basic models, an absorbed optically thin thermal plasma or an absorbed non-thermal power law. Table 2 lists the resulting parameters of the spectral fitting for each object.

3.2. UVOT data

Swift detected the vast majority of our survey sources – 36 out of 41 – in the UV. UV Aur, RW Hya, StH α 190 saturated the UVOT detector so no useful UV data are available. V850 Aql, V503 Her, StH α 55 and NSV 05572 were not detected with a 3σ upper limit of $m_{\text{UV}M2} \gtrsim 21.95$. SWIFT J171951.7-300206 lies inside the saturated-PSF wings of a nearby (approximately 10 arcsec away) source and only was detectable after combining the individual exposures during each visit, thus we only list the average count rates in Table 3. Of the 33 sources with non-saturated UV detections, 21 displayed rapid variability with an rms amplitude more than twice that expected from Poisson statistics alone in at least one UV light curve segment; the rms amplitudes for these sources with unambiguous UV variability ranged from a few percent to more than 20%. For the other 12 sources with non-saturated UV detections, the rms variability amplitude was poorly constrained in some cases (i.e., when the count rate was low), but constrained to be less than a percent or so for others. Comparing the UV variability amplitude with the X-ray hardness ratio revealed that sources with the hardest X-ray spectra have the largest UV variability amplitudes. The observed and expected standard deviations, the fractional rms variability amplitudes and upper limits are listed in Table 3.

4. Individual objects.

4.1. NQ Gem

NQ Gem is listed as a suspected symbiotic star in the catalogue of Belczyński et al.. It shows a ratio of SiIII]/CIII] that is similar to that of other symbiotic stars. An orbital solution was presented by Carquillat & Priour (2008), who found a period of 1308 days, an eccentricity $e=0.182$, and a lower limit on the white dwarf mass of $0.6 M_{\odot}$. The similarity of the optical spectra of NQ Gem and T CrB was noted by Greene & Wing (1971).

The X-ray spectrum of NQ Gem clearly shows two components at energies above and below ≈ 1.5 keV, respectively. This spectrum bears a striking resemblance to that of the well-known WD symbiotic CH Cyg (Mukai et al. 2007). Because of this similarity, we applied an analogous model. We fit the spectrum with a hard thermal component ($kT_1 \gtrsim 16$ keV) seen through a simple absorber ($n_{H,1}=9.0^{+1.9}_{-1.7} \times 10^{22} \text{ cm}^{-2}$) and the soft compo-

Table 1. Observing Log. List sorted by estimated distance (see Section 2), from the nearest to the farthest away.

	Object	Exposure time [ks]	Observation Dates
1	NQ Gem	10.1	2010-04-30
2	UV Aur	14.5	2010-04-13/14/20
3	RW Hya	7.5	2010-05-30/08-02
4	TX CVn	11.5	2010-04-08/21/05-05/18
5	ZZ CMi	11.7	2010-05-02/04/14
6	AR Pav	9.6	2010-05-20/25
7	ER Del	10.6	2010-04-16
8	CD -27 8661	9.0	2010-08-24/26
9	V627 Cas	10.6	2010-04-12/13
10	Hen 3-461	10.0	2010-04-11
11	WRAY 16-51	9.3	2010-07-25/10-11/13
12	SY Mus	10.4	2010-04-07/10/11
13	CD -283719	10.3	2010-04-17
14	V443 Her	9.4	2010-05-25/07-01/03
15	BD -21 3873	10.2	2010-08-22/12-24/26/28
16	NSV 05572	10.3	2010-08-01/11-19
17	V503 Her	9.5	2010-06-04
18	V748 Cen	11.0	2010-09-23, 2011-01-29
19	UKS Ce-1	11.4	2010-06-26/07-06
20	YY Her	9.2	2010-05-23/26/06-05/06
21	StH α 190	9.8	2010-04-03/07/13
22	CI Cyg	18.8	2010-05-02/06-08/09
23	FG Ser	9.7	2010-10-07/09
24	WRAY 15-1470	10.2	2010-06-26/29/10-13, 2011-02-01/02
25	Hen 3-863	9.9	2010-04-13/14/15/18/21/05-04/10
26	AS 210	9.9	2011-02-01/02
27	StH α 32	9.9	2010-04-04
28	V835 Cen	10.1	2010-04-19/21/05-18/21
29	BI Cru	10.8	2010-04-11/14/15/19
30	AS 289	8.1	2010-07-20/31/08-03
31	V850 Aql	9.8	2010-05-30/06-18
32	V347 Nor	15.7	2010-04-14/16/19/05-02/21
33	AX Per	9.4	2010-04-06
34	Hen 3-1213	8.4	2010-04-30/05-21/26
35	LT Del	9.3	2010-06-18/21/23/
36	Y Cra	9.9	2010-05-26/06-24
37	AS 327	11.0	2010-10-29/11-02/03/06
38	StH α 55	16.5	2010-04-14/15/17/20/21
39	KX Tra	10.6	2010-05-22/25
40	V366 Car	8.6	2010-10-08
41	SWIFT J171951.7-300206	10.5	2012-02-01/02/06/08/12

ment with an absorbed ($n_{H,2} \lesssim 0.1 \times 10^{22} \text{cm}^{-2}$) low-temperature plasma ($kT_2=0.23^{+0.03}_{-0.03}$ keV). The unabsorbed flux is $F_X[0.3-10 \text{ keV}]=6.8 \times 10^{-12} \text{ ergs cm}^{-2} \text{ s}^{-1}$, and the luminosity at 1 kpc (the actual distance is unknown) is $L_X=8.1 \times 10^{32} \text{ erg s}^{-1} (d/1 \text{ kpc})^2$.

4.2. UV Aur

The UV Aur system is composed by UV Aur A, a carbon Mira-type variable that is approximately $3.4''$ from UV Aur B, a B8.5-type star (Herbig 2009). Our UVOT observation of UV Aur saturated the detector, which saturates for sources brighter than approximately 7.4 visual magnitudes. As UV Aur A has a magnitude in the range of 7.4-10.6 while UV Aur B has a magnitude of about 11.5 (Herbig 2009), we conclude that the UVOT detected UV Aur A instead of UV Aur B. UV Aur A has been classified as a symbiotic star after the detection of [O III], [Ne III] and [Fe VII] (Sanford 1949, 1950; Seal 1988; Ikeda & Tamura 2004). Given that He II λ 4686 Å has not been yet detected, UV Aur A would not be qualified as a normal symbiotic (Herbig 2009). However the fact that the emission lines of [O III], etc. were

ever detected, is evidence that UV Aur A is likely a symbiotic system.

The X-ray spectrum shows two components, with most of the flux concentrated in the soft component. We model the softer region of the spectrum with a weakly absorbed ($n_{H,1} \lesssim 10^{20} \text{cm}^{-2}$) two-temperature plasma ($kT_1 \lesssim 0.12 \text{ keV}$; $kT_2=0.6^{+0.3}_{-0.1}$ keV) and the hard region was modeled with a heavily absorbed ($n_{H,2}=5.3^{+9.1}_{-3.7} \times 10^{22} \text{cm}^{-2}$) plasma ($kT_3 \gtrsim 2 \text{ keV}$). The unabsorbed flux is $F_X=1.5 \times 10^{-12} \text{ ergs cm}^{-2} \text{ s}^{-1}$. At a distance of 1 kpc (Herbig 2009), the unabsorbed X-ray luminosity is $L_X=1.8 \times 10^{32} \text{ erg s}^{-1} (d/1 \text{ kpc})^2$.

4.3. ZZ CMi

Although Belczyński et al. were ambivalent about whether ZZ CMi is a symbiotic star, the similarities between the properties of the X-ray and UV emission from ZZ CMi and those of other, well-established WD symbiotics leads us to conclude that it is indeed a WD symbiotic. Belczyński et al. noted that the optical colors do not evolve like those of other symbiotics, that the optical emission line strengths are unusual ($H\gamma > H\beta$), and that

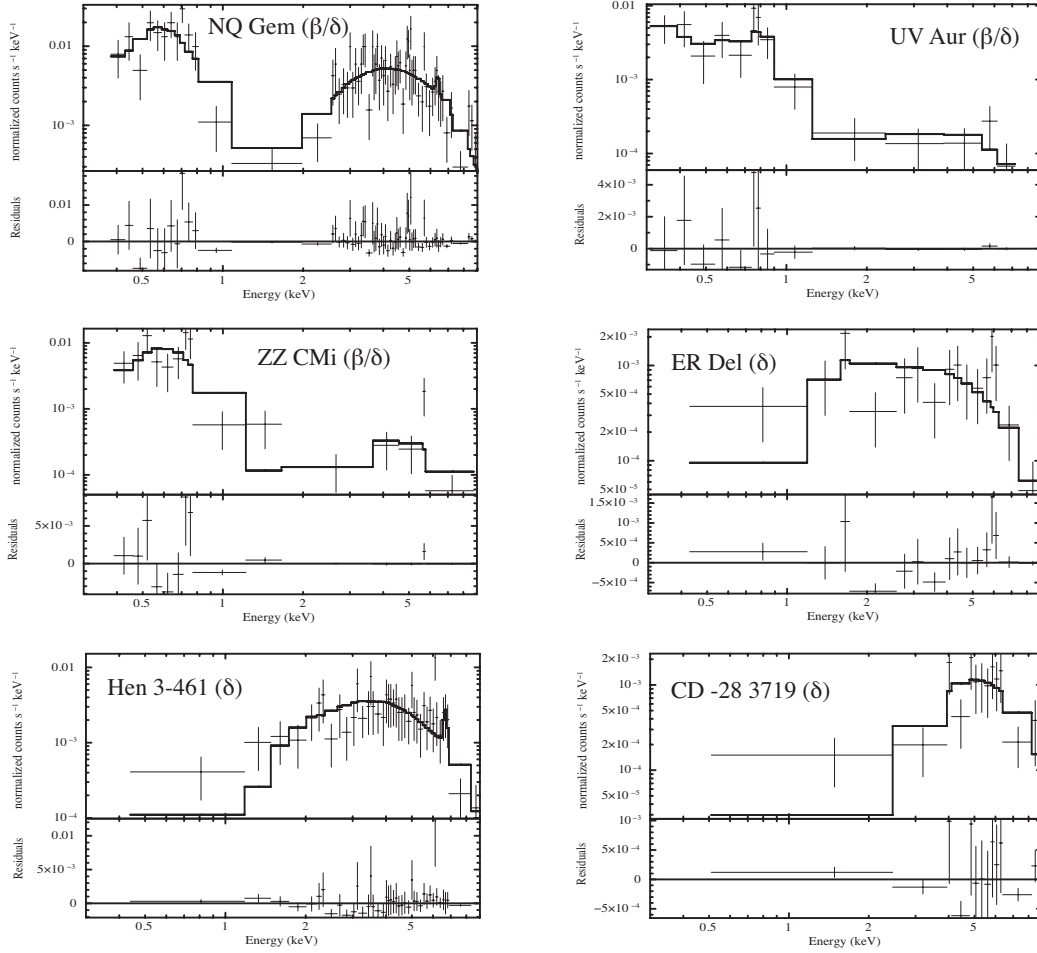


Fig. 1. *Swift*/XRT spectra of the WD symbiotics with newly discovered X-ray emission together with their X-ray spectral types: NQ Gem, UV Aur, ZZ CMi, ER Del, Hen 3-461, CD-28 3719. Full line shows the best fit model as described in Section 3. The X-ray spectral classification for each source is included between parenthesis in each panel and listed in Table 4

the maximum ionization potential could be as low as 35.1 eV. But the source definitely contains a late-type star and displays an emission-line optical spectrum, and the $H\alpha$ profile is similar to that of other WD symbiotics. Since some WD symbiotics with very hard X-ray spectra can have optical spectra that appear to be only “weakly” symbiotic, ZZ CMi could provide another example of the different views of WD symbiotics provided by X-ray and optical observations.

As in the case of NQ Gem, the X-ray spectrum from ZZ CMi closely resembles the spectrum from CH Cyg, with two components primarily above and below ≈ 2 keV, respectively. Therefore we applied a similar spectral model to the one used for NQ Gem consisting of a weakly absorbed ($n_{H,1} \lesssim 0.2 \times 10^{22} \text{ cm}^{-2}$) optically thin thermal plasma ($kT_1 = 0.22^{+0.04}_{-0.05}$ keV) to model the softer energies plus an absorbed ($n_{H,2} = 14^{+19}_{-10} \times 10^{22} \text{ cm}^{-2}$) optically thin plasma ($kT_2 \gtrsim 2.7$ keV) at higher energies. The unabsorbed flux is $F_X = 4.7 \times 10^{-13} \text{ ergs cm}^{-2} \text{ s}^{-1}$, and the luminosity at 1 kpc is $L_X = 5.6 \times 10^{31} \text{ ergs s}^{-1} (d/1 \text{ kpc})^2$.

4.4. ER Del

Although the spectral type of the cool component in ER Del is S5.5/2.5 (Ake 1979), which is relatively rare for a symbiotic star (Van Eck & Jorissen 2002), the optical and UV emission lines (Belczyński et al. 2000) support a symbiotic-star classifi-

cation. In symbiotic stars that contain S stars, the ZrO bands in the spectrum of the red giant indicate that red giant has been polluted by mass transfer from the companion (Van Eck & Jorissen 1999). The UV emission lines have ionization potentials as high as 47.9 eV, and the optical spectrum shows emission lines of H (Belczyński et al. 2000). Moreover, Jorissen et al. (2012) recently determined an orbital period for ER Del of 2089 ± 6 d. These features would suggest that ER Del is indeed a symbiotic binary.

The small number of photons detected (35 photons in a 10.6 ks exposure time) did not allow us to perform an accurate model fit. We applied a simple model consisting of an absorbed ($n_H = 2^{+11}_{-1} \times 10^{22} \text{ cm}^{-2}$) optically thin thermal plasma ($kT \gtrsim 10$ keV). Although the temperature of the plasma is not tightly constrained, the thermal nature of the emission is suggested by the fit residuals at approximately 1.5 and 6 keV, which are probably from emission lines of Mg and Fe respectively. The unabsorbed flux is $F_X = 5 \times 10^{-13} \text{ ergs cm}^{-2} \text{ s}^{-1}$, and the luminosity at 1 kpc is $L_X = 6 \times 10^{31} \text{ ergs s}^{-1} (d/1 \text{ kpc})^2$. The large value of the absorbing column is indicated by the low count rate below ≤ 2 keV.

4.5. Hen 3-461

Hen 3-461 was classified as a suspected symbiotic in the catalog of Allen (1984). Its optical spectrum shows a late-type con-

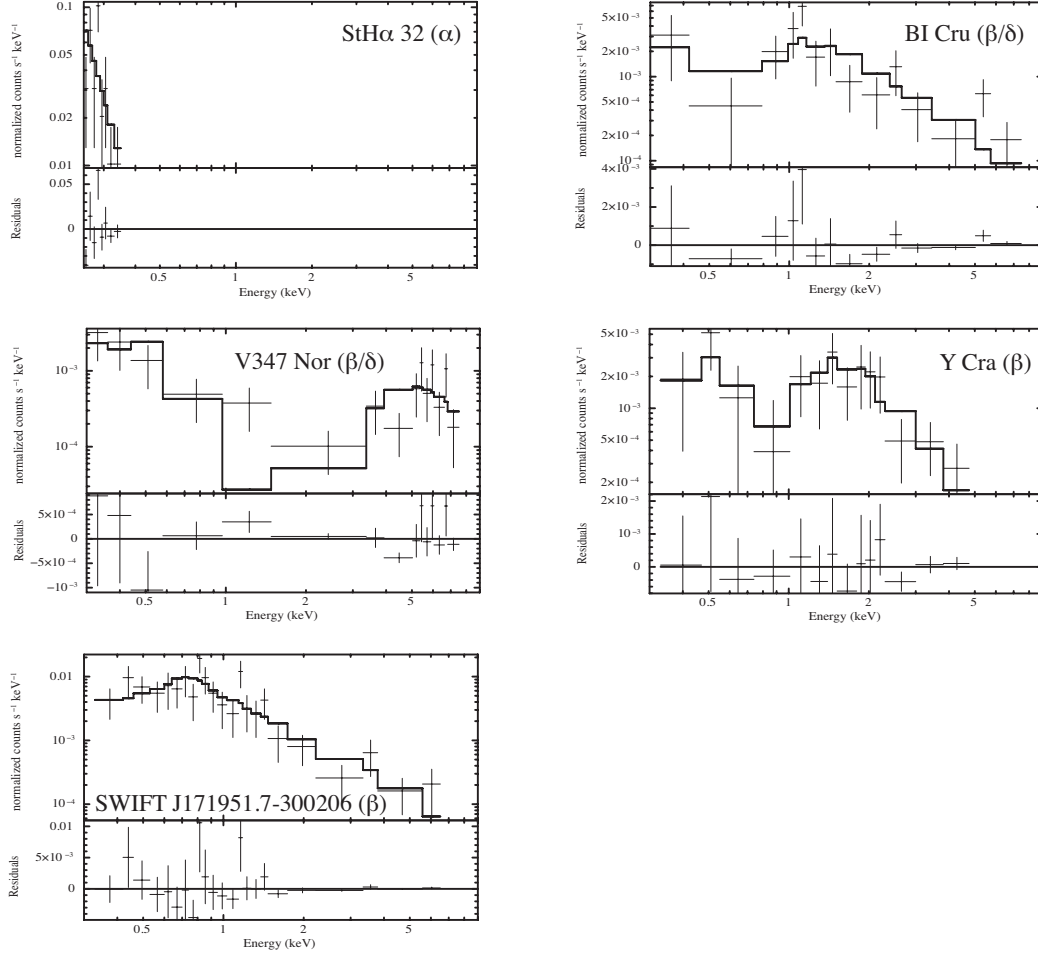

Fig. 2. Same as Figure 1 for StH α 32, BI Cru, V347 Nor, Y Cra and SWIFT J171951.7-300206.

Table 2. X-ray spectral fitting results.

Object	Model	n_H cm $^{-2}$ [10^{22} cm $^{-2}$]	kT [keV]	$F_X[0.3-10$ keV] [10^{-13} ergs s $^{-1}$ cm $^{-2}$]	L_X [10^{31} ergs s $^{-1}$]	
1	NQ Gem	wabs $_1$ \times apec $_1$ +wabs $_2$ \times apec $_2$	1: ≤ 0.1 2: $9.0^{+1.9}_{-1.7}$	1: $0.23^{+0.03}_{-0.03}$ 2: ≥ 16	68	81 (d/1 kpc) 2
2	UV Aur	wabs $_1$ \times (apec $_1$ +apec $_2$)+wabs $_2$ \times apec $_3$	1: ≤ 0.01 2: $5.3^{+9.1}_{-3.7}$	1: ≤ 0.12 ; 2: $0.6^{+0.3}_{-0.1}$ 3: ≥ 2	15	18 (d/1 kpc) 2
5	ZZ CMi	wabs $_1$ \times apec $_1$ +wabs $_2$ \times apec $_2$	1: ≤ 0.2 2: 14^{+19}_{-10}	1: $0.22^{+0.04}_{-0.05}$ ≥ 2.7	4.7	5.6 (d/1 kpc) 2
7	ER Del	wabs \times apec	≥ 11	≥ 10	5	6 (d/1 kpc) 2
10	Hen 3-461	wabs \times apec wabs \times pcfabs \times (mckflow)	$6.1^{+2.4}_{-1.6}$ full= $2.0^{+2.5}_{-1.3}$ partial= 10^{+6}_{-5} cf= $0.87^{+0.10}_{-0.30}$	$7.6^{+11.8}_{-3.4}$ ≥ 3.4	38 62	45 (d/1 kpc) 2 74 (d/1 kpc) 2
13	CD -283719	wabs \times apec	≥ 11	≥ 11	25	30 (d/1 kpc) 2
27	StH α 32	bbbody	...	$0.03^{+0.02}_{-0.01}$	9	10 (d/1 kpc) 2
29	BI Cru	wabs $_1$ \times apec $_1$ +wabs $_2$ \times apec $_2$	1: ≤ 0.1 2: ≤ 0.6	≤ 0.17 ≥ 1.9	3.2	15 (d/2 kpc) 2
32	V347 Nor	apec $_1$ +wabs \times apec $_2$	≥ 16	$0.15^{+0.06}_{-0.05}$ ≥ 2.5	48	150 (d/1.5 kpc) 2
36	Y Cra	wabs $_1$ \times apec $_1$ +wabs $_2$ \times apec $_2$	1: ≤ 0.6 2: $1.6^{+0.4}_{-0.3}$	1: ≤ 0.3 2: $1.3^{+0.4}_{-0.3}$	12	14 (d/1 kpc) 2
41	SWIFT J171951.7-300206	wabs \times (apec $_1$ +apec $_2$)	≤ 0.1	$1.0^{+0.1}_{-0.1}$ 2: ≥ 3	2	95 (d/6.3 kpc) 2

tinuum with prominent TiO bands and emission lines from the Balmer series, He I, [Ne III], [O III] and [FeVII]. The optical spectrum of Hen 3-461 resembles the spectrum of RT Cru and T CrB in quiescence (Pereira et al. 1998), with a strong red continuum and weak Balmer lines. Little is known about this source at other wavelengths.

The X-ray spectrum of Hen 3-461 (Figure 1) is similar to the one from RT Cru in that it consist of a highly absorbed, strong continuum extending to high energies. Assuming a simple model consisting of an absorbed, optically thin thermal plasma, we find $n_H = 6.1^{+2.4}_{-1.6} \times 10^{22}$ cm $^{-2}$ and $kT = 7.6^{+11.8}_{-3.4}$ keV. This model has a unabsorbed flux $F_X = 3.8 \times 10^{-12}$ ergs cm $^{-2}$ s $^{-1}$. Taking a more complex model, similar to RT Cru and T CrB

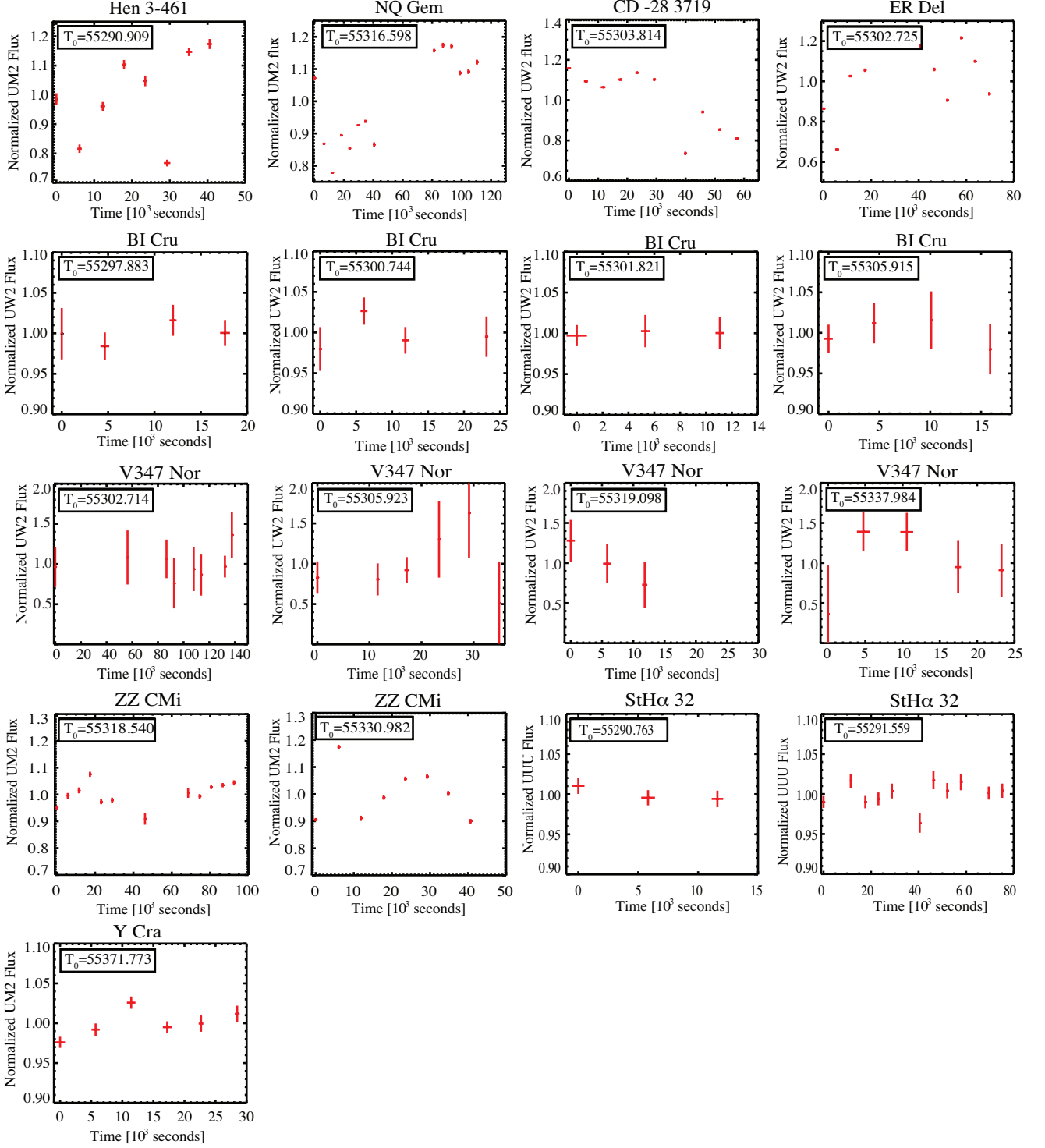


Fig. 3. *Swift* UVOT light curves of X-ray detected sources (except for UV Aur that saturated the UVOT detector, see Section 3). We show the starting time of the observation, T_0 , in units of MJD. The x-axis has units of 10^3 seconds after T_0 . Those visits with less than 3 exposures are not shown.

(Luna & Sokoloski 2007; Luna et al. 2008), which consists of an absorbed multi-temperature cooling flow plasma, we find a lower limit for the maximum temperature for the cooling flow component of $kT_{max} \gtrsim 3.4$ keV and solar abundances (Anders & Grevesse 1989). In the complex model, the absorber has two components, one that completely covers the X-ray source

($n_H(\text{full})=2.0^{+2.5}_{-1.3} \times 10^{22} \text{ cm}^{-2}$) and one that only partially covers it ($n_H(\text{partial})=10^{+6}_{-5} \times 10^{22} \text{ cm}^{-2}$, with a covering fraction of $0.87^{+0.10}_{-0.30}$). Assuming a distance of 1 kpc, the resulting mass accretion rate is $\dot{M} \lesssim 4 \times 10^{-9} M_{\odot}/\text{yr} (d/1 \text{ kpc})^2$. The measured

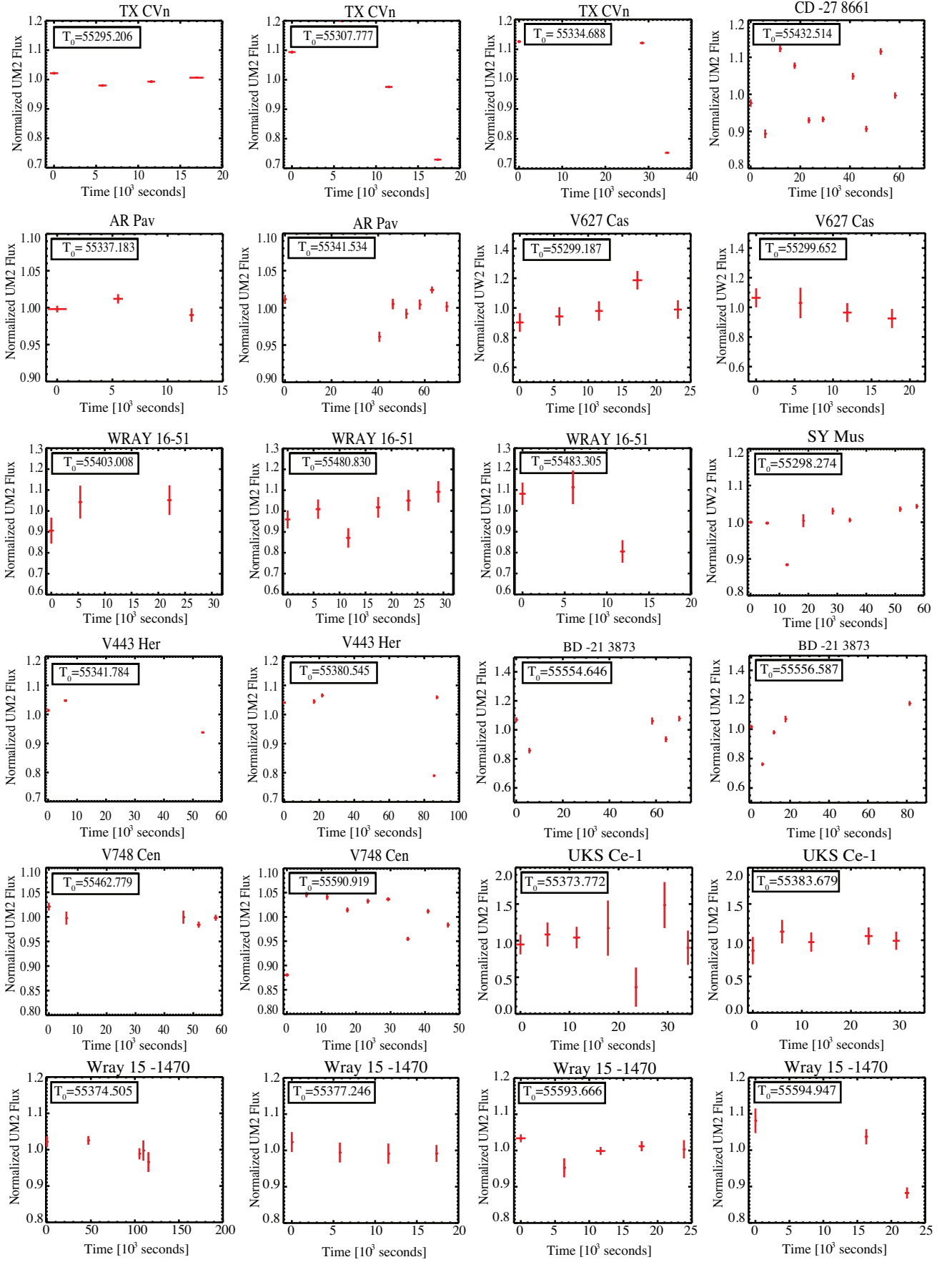


Fig. 4. *Swift* UVOT light curves of source that did not produce detectable X-ray emission. We show the starting time of the observation, T_0 , in units of MJD. The x-axis has units of 10^3 seconds after T_0 . Those visits with less than 3 exposures are not shown.

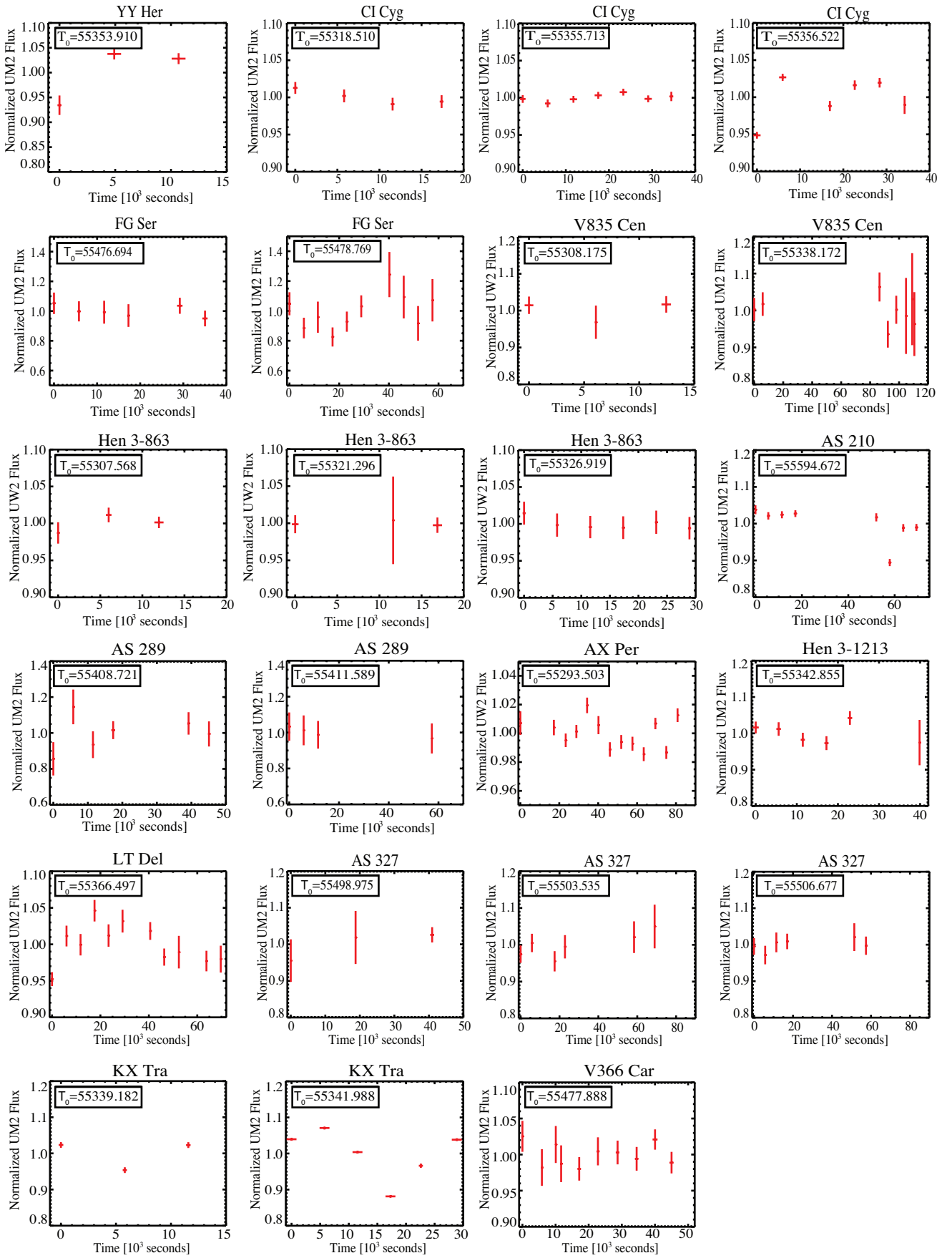


Fig. 5. Same as Figure 4

unabsorbed flux is $F_X=6.2\times 10^{-12}$ ergs cm^{-2} s^{-1} and hence the luminosity is $L_X=7.4\times 10^{32}$ ergs s^{-1} ($d/1$ kpc) 2 .

4.6. CD -28 3719

The symbiotic nature of CD -28 3719 has been suggested based on its broad $H\alpha$ profiles and blue colors (Belczyński et al. 2000 and references therein). With an exposure time of 10.2 ks, we detected 30 X-ray photons from CD -28 3719. We fit the spectrum with a simple model composed of a highly absorbed ($n_H = 29^{+20}_{-12}\times 10^{22}$ cm^{-2}) plasma with a temperature of $kT \gtrsim 11$ keV. The unabsorbed flux is $F_X=2.5\times 10^{-12}$ ergs cm^{-2} s^{-1} , and the luminosity at a distance of 1 kpc is $L_X=3\times 10^{32}$ ergs s^{-1} ($d/1$ kpc) 2 . Although the low number of photons precludes a more precise fit, the lower limit on n_H requires the spectrum to be highly absorbed.

4.7. StH α 32

StH α 32 is a known supersoft source (Orio et al. 2007) and it was included by accident in our target list. However, no X-ray spectrum has been published in the literature until now. Haakonsen & Rutledge (2009) determined a probability of 0.721 for StH α 32 to be associated with the symbiotic source 2MASS J0437456-0119118. StH α 32 belongs to the small group of barium-rich symbiotics, i.e. systems that exhibit symbiotic features such as H I and He II in their optical and UV spectra and barium star type abundance anomalies (Schmid 1994).

Given that *Swift*/XRT detected only 31 photons from StH α 32, all with energies less than or equal to 0.4 keV, we only obtained approximated values for the parameters of the spectral model. We fit the spectrum with blackbody model with a temperature of $kT=0.03^{+0.02}_{-0.01}$ keV. The flux is $F_X=9\times 10^{-13}$ ergs cm^{-2} s^{-1} and at a distance of 1 kpc, the luminosity is $L_X=4\times 10^{32}$ ergs s^{-1} ($d/1$ kpc) 2 . Most known supersoft sources have luminosities in the 10^{35-36} ergs s^{-1} range (see, e.g. Orio et al. 2007), therefore it is possible that StH α 32 is farther away, likely in the galactic halo, as proposed by Schmid & Nussbaumer (1993) based on the small reddening toward the source, its galactic coordinates ($l = 197^\circ$, $b = -30^\circ$) and radial velocity (v_r 325 km s^{-1}).

4.8. BI Cru

The symbiotic system BI Cru is comprised of a Mira-type red giant with a pulsation period of 280 days, an accreting white dwarf, and a bipolar nebula that extend 1.3 pc from the central binary perpendicular to the orbital plane (Contini et al. 2009). The bipolar structures (expanding at ≈ 200 km s^{-1}) could be explained by the presence of an accretion disk and periodic hydrogen shell flashes on the surface of the white dwarf (with flashes every ~ 1000 yr; Corradi & Schwarz 1993). In their model of an optical spectrum taken in 1974, Contini et al. (2009) proposed that shocks in the inner nebula (from an unrecorded outburst) could be fast enough, with speeds of a few thousands km s^{-1} , to produce X-ray emission. If these shocks produce the X-ray emission that we have observed, they must either not have had time to cool or have been fed by more recent mass ejections.

The X-ray spectrum obtained with *Swift* shows two apparently distinct components at low and high energies. We fit the X-ray spectrum with a model consisting of a two-temperature plasma. The cooler plasma ($kT_1 \lesssim 0.17$ keV) is slightly absorbed ($n_{H,1} \lesssim 0.1 \times 10^{22}$ cm^{-2}), while the plasma that produce the harder emission ($kT_2 \gtrsim 1.9$ keV) is seen through moder-

ate absorption ($n_{H,2} \lesssim 0.6 \times 10^{22}$ cm^{-2}). The total unabsorbed flux is $F_X=3.2\times 10^{-13}$ ergs cm^{-2} s^{-1} and at a distance of 2 kpc (McCollum et al. 2008), the luminosity is $L_X=1.5\times 10^{32}$ ergs s^{-1} ($d/2$ kpc) 2 . The hard component accounts for approximately 95% of the flux. The detection of the soft component is dubious, as the background also peaks at these energies and it is not well sampled in our short observation.

4.9. V347 Nor

V347 Nor is a symbiotic with a Mira-type red giant (Belczyński et al. 2000). It shows an extended nebula discovered by Munari & Patat (1993). Santander-García et al. (2007) determined a distance of 1.5 ± 0.4 kpc using the expansion parallax method. Based on the similarity of the X-ray spectrum with CH Cyg, we fit the X-ray spectrum with a two-component model. We used two optically thin thermal plasmas; a low temperature plasma ($kT_1=0.15^{+0.06}_{-0.05}$ keV) and a highly absorbed ($n_H \gtrsim 16\times 10^{22}$ cm^{-2}) high temperature plasma ($kT_2 \gtrsim 2.5$ keV). The unabsorbed flux is $F_X=4.8\times 10^{-12}$ ergs cm^{-2} s^{-1} , and the luminosity at 1.5 kpc is $L_X=1.3\times 10^{33}$ ergs s^{-1} ($d/1.5$ kpc) 2 .

4.10. Y Cra

Luna & Costa (2005) carried out a detailed optical spectroscopic study of this source, and placed constraints on the physical conditions of the nebula, i.e. electronic density, E(B-V), Ne/O and Ar/O abundance ratios. Nussbaumer et al. (1988) determined C/N and O/N abundance ratios using IUE data. In this regard, Y Cra does not stand out as a particularly unusual source.

During our program, all objects other than Y Cra were detected in X-rays at the position (J2000 epoch) listed in the catalogue of Belczyński et al. (2000). In the Y Cra field, an X-ray source is detected at $\alpha=18\text{h } 14\text{m } 20.425\text{s}$, $\delta=-42^\circ 50' 22.143''$, while the coordinates from Belczyński et al. catalogue are $\alpha=18\text{h } 14\text{m } 22.951\text{s}$, $\delta=-42^\circ 50' 32.40''$. This discrepancy in position is approximately 10 times the radius of the *Swift*/XRT error circle (which is about 3 arcsec). Nonetheless, as SIMBAD does not list any other source near either position, we tentatively identify this X-ray source as the WD symbiotic Y Cra.

We model the spectrum with two independently absorbed thermal components. The absorption of the low-temperature component ($kT_1 \lesssim 0.3$) is not tightly constrained by the fit ($n_{H,1} < 0.6\times 10^{22}\text{cm}^{-2}$). The high-temperature component ($kT_2=1.3^{+0.4}_{-0.3}$ keV) in turn is affected by moderate absorption ($n_{H,2} = 1.6^{+0.4}_{-0.3}\times 10^{22}\text{cm}^{-2}$). The unabsorbed flux is $F_X=1.2\times 10^{-12}$ ergs cm^{-2} s^{-1} , and the luminosity at a distance of 1 kpc is $L_X=1.4\times 10^{32}$ ergs s^{-1} ($d/1$ kpc) 2 .

4.11. SWIFT J171951.7-300206, a newly discovered symbiotic in the field of IGR J17197-3010.

On February 2012, *Swift*/XRT detected an X-ray source at the coordinates $\alpha = 17\text{h } 19\text{m } 51.7\text{s}$ and $\delta=-30^\circ 02' 0.6''$ (Luna et al. 2012, with an error radius of $4.3''$). These XRT coordinates are consistent with the position of a symbiotic star at $\alpha=17\text{h } 19\text{m } 51.83\text{s}$ and $\delta=-30^\circ 02' 0.3''$ (Masetti et al. 2012). We therefore use the *Swift* naming convention and refer to this symbiotic hereafter as SWIFT J171951.7-300206. Although Masetti et al. (2012) proposed that this symbiotic star might be the counterpart to the γ -ray source IGR J17197-3010, Luna et al. (2012) concluded that the location of the two X-ray sources in the *Swift*/XRT field of the γ -ray source did not support the associa-

tion between the symbiotic star and the γ -ray source. Therefore, although WD symbiotics have been known to produce γ rays (e.g., Masetti et al. 2005), SWIFT J171951.7-300206 appears unlikely to have done so.

The XRT spectrum of SWIFT J171951.7-300206 extends up to approximately 5 keV. We model the spectrum with an absorbed ($n_H \lesssim 0.1 \times 10^{22} \text{ cm}^{-2}$) two-temperature plasma ($kT^1 = 0.3^{+0.1}_{-0.1} \text{ keV}$ and $kT^2 \gtrsim 3 \text{ keV}$). The unabsorbed flux is $2 \times 10^{-13} \text{ ergs cm}^{-2} \text{ s}^{-1}$, and at a distance of 6.3 kpc (Masetti et al. 2012), the X-ray luminosity is $L_X = 9.5 \times 10^{32} \text{ ergs s}^{-1} (d/6.3 \text{ kpc})^2$

5. Discussion and conclusions

We find that the X-ray spectra of newly discovered X-ray sources fall naturally into three groups. The first comprises those sources with highly absorbed, hard ($E \gtrsim 2 \text{ keV}$) single component X-ray spectra. The second includes sources with two distinct X-ray spectral components, one soft ($E \lesssim 2 \text{ keV}$) and one hard. The last group is made up of sources with soft, single-component X-ray spectra. As the α , β and γ categorization introduced by Muerstet et al. (1997) was based on ROSAT data, it naturally missed those WD symbiotics with hard, highly absorbed X-ray spectra. Moreover, the hard component of those systems with both soft and hard X-ray spectral components were also not detectable with ROSAT, and two-component X-ray spectra were thus also not included in this scheme.

We therefore propose an updated classification scheme for the X-ray spectra of symbiotic stars that builds upon and extends the previous scheme proposed by Muerstet et al. (1997). We retain their α , β , and γ X-ray spectral classes and introduce a new category – δ – to identify those WD symbiotics with hard, highly absorbed X-ray spectra. Since WD symbiotics with both soft and hard components in their X-ray spectra share features of the β - and δ -types, we dub these systems β/δ . We summarize the new groups as:

- α : Supersoft X-ray sources with most of the photons having energy less than 0.4 keV. The likely origin is quasi-steady shell burning on the surface of the white dwarf.
- β : Soft X-ray sources with most of the photons having energy less than 2.4 keV, the maximum energy detectable with ROSAT. The likely origin is the collision of winds from the white dwarf with those from the red giant.
- γ : Symbiotic stars with neutron-star accretors, also known as symbiotic X-ray binaries. Their X-ray spectra extend toward high energies ($E \gtrsim 2.4 \text{ keV}$) and can be modeled as due to optically thick Comptonized plasma with no emission lines.
- δ : Highly absorbed, hard X-ray sources with detectable thermal emission above 2.4 keV. The likely origin is the boundary layer between an accretion disk and the white dwarf.
- β/δ : WD symbiotics with two X-ray thermal components, soft and hard. They share features of β and δ types. The soft emission is likely produced in a colliding-wind region, and the hard emission is likely produced in an accretion-disk boundary layer.

In Table 4 we show the classification, under the new scheme, of all the symbiotics that have reported X-ray detections. Some classifications are uncertain due to the short exposure time of our exploratory survey and are labeled as such in Table 4. Figure 6 shows X-ray hardness (as defined in Section 3) as a function of XRT count rate for the WD symbiotics with newly detected X-ray emission as well as those with previously known δ -type

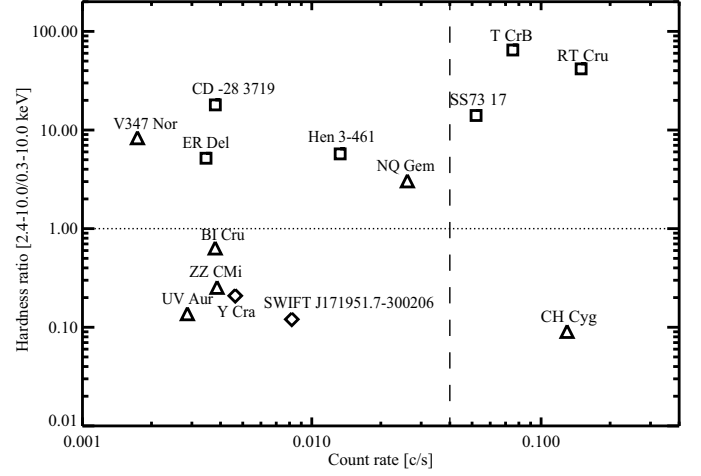


Fig. 6. Hardness ratio vs count rate in counts s^{-1} for the hard X-ray WD symbiotics that have been observed with *Swift*. The newly X-ray detected WD symbiotics are all located to the left of the dashed line, confirming that because of their low fluxes, they were not detected before. The plot shows that δ -type sources (\square) have *Hardness ratio* of more than 1 (above the dotted horizontal line); β -type sources (\triangle) have *Hardness ratio* of less than 1 while β/δ -type sources (\diamond) are located above and below the *Hardness ratio* = 1 line. Hence, accretion-dominated δ -type objects lie above *Hardness ratio* \approx 1, while below this line we find soft X-ray sources, whose X-ray spectrum is dominated by emission originated in a colliding-wind region.

emission. As expected, the sources with newly detected X-ray emission have lower fluxes than the prior discoveries, confirming that they were not detected in various previous X-ray surveys because they were too faint. We can also see in this figure that there are basically two regions, above and below *Hardness ratio* \approx 1, that separates δ -type from β and β/δ -type objects.

Taking distance estimates into account, the detection rate of X-ray emission from WD symbiotics with *Swift*/XRT indicates that faint X-ray emission is a common, but not universal, property of symbiotic stars. Symbiotic stars constitute an important and growing population of X-ray sources (44 objects), with 7 sources showing supersoft emission, 12 sources with soft thermal X-ray emission, 8 sources with soft and hard thermal X-ray emission, 6 sources with hard thermal X-ray emission, and 11 sources with hard non-thermal X-ray emission from accretion onto a neutron star. Since 6 of our 11 *Swift* X-ray detections came from the top 13 of the 41 on our fill-in target list (i.e., $\sim 2/3$ of our detections are from the top third of our list), which was sorted by rough distance estimate, some of the non-detected objects could have similar X-ray emission as the detections, but just be farther away. For example, the β/δ system CH Cyg would be categorized as δ -type if it was 10 times farther away and is observed during a high-flux state (the distance of CH Cyg is 245 pc and its flux varies between high and low states; Mukai et al. 2007). During a low-flux state it would not be detected in a survey like the one presented here. The distance, however, cannot be the only factor in whether or not the XRT detected a source, because we did not detect, e.g. SY Mus, CI Cyg and RW Hya, with distances of 0.76, 1.5 and 0.68 kpc respectively (Muerstet et al. 1991).

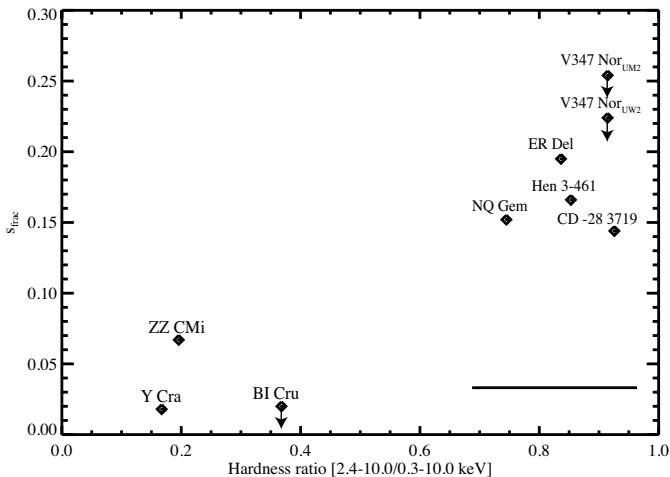


Fig. 7. Fractional rms amplitude of rapid UV variability (s_{frac}) vs ratio of hard (2.4–10.0 keV) to total (0.3–10.0 keV) X-ray count rates. Objects with harder X-ray spectra tend to have more intense UV variability. Since rapid variability is a hallmark of accretion, this trend supports our proposition that the hard X-ray emission in WD symbiotics is powered by accretion. V347 Nor was observed with two UV filters, and we plot the fractional variability from each of the observations. Downward arrows indicate upper limits. Average errorbar is shown at the bottom-right corner.

5.1. β -type emission

We suggest that the β -type spectrum is from shock-heated plasma due to colliding winds. Two basic models have been proposed to explain the β -type emission from WD symbiotics: 1) colliding winds from the WD and red giant (Muerset et al. 1997; Mukai et al. 2007); and 2) scattering of hard X-ray photons from near the surface of the WD into our line of sight (Wheatley & Kallman 2006). The scattering model proposed by Wheatley & Kallman (2006), however, required that the binary be seen almost edge-on. Since it is unlikely that all 5 of the new two-component WD symbiotics are edge-on, the *Swift* data support the colliding winds model over the scattering model for the β component in the X-ray spectra for WD symbiotics. From our survey, Y Cra and SWIFT J171951.7–300206 have a β -type spectra originated in a colliding-wind. The temperatures obtained from spectral models of the soft component (a few MK) suggest plasma heated by shocks at speeds of a few hundreds km s^{-1} , which are roughly consistent with the speeds of outflows from WD symbiotics (Nichols et al. 2007; Galloway & Sokoloski 2004). The luminosity from this colliding wind region for the new objects and CH Cyg are all commensurate (see Mukai et al. 2007), with $L_X[0.3 - 2.4 \text{ keV}] \sim 10^{30-31} \text{ ergs s}^{-1}$. Since $L_X \propto \int n^2 dV/d^2$, where n is the density, V is the volume of the emitting region and d is the distance to the source, then the amount of emitting material, i.e. the emission measure of the new sources, has to be a few times larger than in CH Cyg.

5.2. δ -type emission

We suggest that the hard X-ray emission in δ and β/δ systems is from the accretion rather than quasi-steady nuclear burning or colliding winds. The high level of absorption of the hard emission shows that these high-energy photons are emitted from well within the symbiotic wind nebula. The lack of any coherent mod-

ulation of the hard X-ray emission supports our idea that the hard emission is not due to magnetic accretion onto a rotating WD (albeit our data are only sensitive to pulsed fractions of more than $\approx 44\%$, see Section 3). The hard X-ray component of the spectrum is well-fit by thermal models with temperatures of a few keV, which are unlikely to be produced in the colliding region of low-velocity winds. The presence of variability on time scales of minutes to hours at UV wavelengths supports the accretion scenario over quasi-steady nuclear burning, which varies on the much longer nuclear timescale. (Sokoloski 2003). Figure 7 shows that sources with the hardest X-ray spectrum (see Figures 1 and 2) are also more UV variable (group at the upper right corner in Figure 7), while sources with low amplitude UV flickering tend to have relatively little emission above 2 keV (lower left corner group). The UVOT light curve from our unintended observation of the supersoft source StH α 32 supports the proposed scenario in which sources powered by nuclear shell burning do not show large amplitude flickering (see Figure 3 lower right panel and Table 3). Moreover, unlike the WD symbiotics that produce δ -type X-ray emission, the X-ray faint sources SY Mus, CI Cyg, and RW Hya all have luminous WDs (a few hundreds to thousands L_\odot ; Muerset et al. 1991) Because the amount of energy released by nuclear burning material exceeds the energy released by accretion, these sources are most likely powered by nuclear-burning material on the surface of their white dwarfs, in contrast to the sources that we detect in hard X-rays, which we believe to be mostly accretion-powered. If the UV flux from any WD with quasi-steady shell burning is strong enough to Compton-cool the plasma in the boundary layer, that would explain the lack of δ -type emission from such WD symbiotics.

The low X-ray fluxes (especially when compared to the UV fluxes) suggest that the boundary layers are predominantly optically thick in most cases. Whereas, the UV-to-X-ray flux ratio is less than 1 from the almost entirely optically thin boundary layer in the δ -type WD symbiotic T CrB ($F_{UV,M2} = 2.3 \times 10^{-12} \text{ ergs cm}^{-2} \text{ s}^{-1}$; $F_X = 1.4 \times 10^{-11} \text{ ergs cm}^{-2} \text{ s}^{-1}$; Luna et al. 2008), it is greater than 10 for all the δ -type sources except for Hen 3-461. Interestingly, the UV-to-X-ray flux ratio for Hen 3-461 is $\lesssim 0.1$, like in T CrB, suggesting that most of its X-ray flux could also originate in a mostly optically thin boundary layer. Moreover, the spectral fit of a cooling flow model yielded a mass accretion rate $\dot{M} \lesssim 4 \times 10^{-9} M_\odot/\text{yr} (d/1 \text{ kpc})^2$ (see Section 4.5), which is within the regime of optically thin boundary layer emission around a $1 M_\odot$ white dwarf as computed by Narayan & Popham (1993). The luminosity of the δ spectral components from the objects listed in Table 2 (modulo uncertainties in the distances) ranges from $10^{31} \text{ ergs s}^{-1}$ (ZZ CMi) to $10^{32} \text{ ergs s}^{-1}$ (V347 Nor). For comparison, the luminosity from the accretion disk boundary layer in T CrB is on the order of $7 \times 10^{33} \text{ ergs s}^{-1} (d/1 \text{ kpc})^2$ (Luna et al. 2008).

Because most of the boundary layers appear to be optically thick, and also because inverse Compton scattering could be cooling the plasma in the boundary layers, we cannot place tight constraints on the masses of the WDs in the symbiotics with newly detected X-ray emission. The hardness of the spectrum depends on the optical depth and temperature of the X-ray emitting plasma (Kylafis & Lamb 1982). The measured temperature can be smaller than the actual shock temperature if all or a significant portion of the boundary layer is optically thick. Compton cooling can dominate over bremsstrahlung cooling when a strong source of UV photons is available and the density is low – a condition that could be met in the immediate post-shock regions if the boundary layer is partially optically thick, or if some nuclear burning is taking place on the surface of

the WD. Compton cooling, therefore lowers the temperature of the observed hard X-ray emission. Compelling evidence of this phenomenon has been presented by Nelson et al. (2011) in their analysis of the quiescent X-ray emission from RS Oph, whose white dwarf is known to be massive and accreting at a high rate, yet has a soft, faint X-ray spectrum compared to that of T CrB, an otherwise similar system. The temperatures derived from the X-ray fits, and the UV fluxes, suggest that this might indeed be the case for the new objects and they could still harbor massive white dwarfs, powered by accretion rather than nuclear shell burning.

The new *Swift*/XRT detections of WD symbiotics do, however, allow us to place rough constraints on the rate of accretion onto the WDs in these systems. If our conclusion that the sources with a δ component are powered by accretion rather than nuclear shell burning is valid, then there is a theoretical upper limit for the accretion rate \dot{M} as a function of the WD mass (see e.g. Iben 1982; Nomoto et al. 2007). If the accretion proceeds through a disk and the boundary layer is optically thick, there is also a theoretical lower limit to \dot{M} (for a particular WD mass; Popham & Narayan 1995). For $M_{WD}=1.0, 0.8$ and $0.6 M_{\odot}$, and for the X-ray emission to be from an optically thick boundary layer, these two theoretical considerations require that \dot{M} is $\sim 10^{-7}$, a few $\times 10^{-8}$ and $\sim 10^{-8} M_{\odot} \text{ yr}^{-1}$ respectively. The lower limit, however, suffers from theoretical uncertainties as it depends on the adopted viscosity parameter α . A change of about 30% in α implies a change of approximately a factor of 3 in the accretion rate at which the transition from optically thin to thick boundary layer occurs. Moreover, Fertig et al. (2011) found that values of α derived from observations of dwarf novae are all much lower than predictions from Popham & Narayan (1995). Regardless of these uncertainties, our data suggest that mass transfer rates on the order of $\sim 10^{-8} M_{\odot} \text{ yr}^{-1}$ are rather common in symbiotics and consistent with expectations from Bondi-Hoyle accretion from the red giant wind.

5.3. β/δ -type X-ray spectra

β/δ -type X-ray spectra are prevalent among the WD symbiotics, and could be associated with the production of bi-polar outflows. The new β/δ systems that we have discovered with *Swift* – BI Cru, NQ Gem, ZZ CMi, V347 Nor and UV Aur – have spectra that resemble the well-known X-ray spectra from the WD symbiotics CH Cyg and R Aqr, suggesting that although this X-ray spectral type was previously thought to be unusual, it is actually common. If these 5 new objects had been observed with ROSAT, they would have been classified as β -type in the scheme of Muerse et al. However, these objects also display a hard X-ray component characteristic of δ -type (see above) systems. Therefore, we revise the (Muerse et al. 1997) classification scheme and categorize two-components X-ray spectra as β/δ type.

An interesting similarity between the recently discovered β/δ -type WD symbiotics V347 Nor and BI Cru, and the previously known β/δ -type CH Cyg and R Aqr is that all have extended, bi-polar outflows (e.g., Corradi et al. 1999). The luminosity of the β component in our newly discovered β/δ -type WD symbiotics, however, is higher than the luminosity of the jet components in CH Cyg and R Aqr. The β components of V347 Nor and BI Cru have luminosities of approximately $5 \times 10^{30} (d/1.5 \text{ kpc})^2$ and $7 \times 10^{30} (d/2 \text{ kpc})^2$ respectively. In turn, the jet component in CH Cyg has a luminosity of $5 \times 10^{28} \text{ ergs s}^{-1} (d/245 \text{ pc})^2$ (Karovska et al. 2007); the NE jet in R Aqr has a luminosity of $7 \times 10^{29} \text{ ergs s}^{-1}$ and the SE jet has a luminosity of $2 \times 10^{29} \text{ ergs s}^{-1}$ (Nichols et al. 2007). Thus, the jet emission

in β/δ -type WD symbiotics is not contributing significantly to the flux of the β component. Moreover, both CH Cyg and R Aqr have spatially unresolved β -type emission that is much stronger than the jet emission. Then, the β -type emission seems to be either from the inner, spatially-unresolved portions of the jet or from some other source of emission that preferentially appears when jets are present. Although not yet observed with sensitive hard X-ray detectors, our findings suggest that V1016 Cyg and HM Sge, both symbiotic binaries with outflows detected in optical, could be also β/δ -type systems.

5.4. Conclusions:

1. X-ray emission is a common feature of WD symbiotics.
2. The X-ray spectra of WD symbiotics show 3 distinct spectral components — α , which is associated with quasi-steady shell burning; β , which is most likely from colliding winds; δ , which we propose is from the innermost accretion region. β - and δ -type X-ray emission are often, but not always, found together.
3. The UV-to-X-ray flux ratio of the δ -type targets reveals that the innermost accretion region, which is probably a boundary layer in most cases, is often optically thick, as expected for $0.6 M_{\odot}$ WDs accreting at the Bondi-Hoyle rate of $\approx 10^{-8} M_{\odot}/\text{yr}$.
4. Although most WD symbiotics do not produce detectable optical flickering on time scales of minutes, rapid UV flickering — presumably associated with accretion — is pervasive.

Acknowledgements. G. J. M. Luna is a member of the CIC-CONICET (Argentina). JLS acknowledge support from grants SAO GO1-12041A and NASA NNX10AK31G.

References

- Ake, T. B. 1979, *ApJ*, 234, 538
 Allen, D. A. 1984, *Proceedings of the Astronomical Society of Australia*, 5, 369
 Anders, E. & Grevesse, N. 1989, *Geochim. Cosmochim. Acta*, 53, 197
 Arnaud, K., Smith, R., & Siemiginowska, A. 2011, *Handbook of X-ray Astronomy*, ed. R. Ellis, J. Huchra, S. Kahn, G. Rieke, & P. B. Stetson
 Arnaud, K. A. 1996, in *Astronomical Society of the Pacific Conference Series*, Vol. 101, *Astronomical Data Analysis Software and Systems V*, ed. G. H. Jacoby & J. Barnes, 17
 Belczyński, K., Mikołajewska, J., Munari, U., Ivison, R. J., & Friedjung, M. 2000, *A&AS*, 146, 407
 Bondi, H. & Hoyle, F. 1944, *MNRAS*, 104, 273
 Bucccheri, R., Bennett, K., Bignami, G. F., et al. 1983, *A&A*, 128, 245
 Carquillat, J.-M. & Prieur, J.-L. 2008, *Astronomische Nachrichten*, 329, 44
 Cash, W. 1979, *ApJ*, 228, 939
 Chernyakova, M., Courvoisier, T. J.-L., Rodriguez, J., & Lutovinov, A. 2005, *The Astronomer's Telegram*, 519, 1
 Chiotellis, A., Schure, K. M., & Vink, J. 2012, *A&A*, 537, A139
 Contini, M., Angeloni, R., & Rafanelli, P. 2009, *MNRAS*, 396, 807
 Corradi, R. L. M., Ferrer, O. E., Schwarz, H. E., Brandi, E., & García, L. 1999, *A&A*, 348, 978
 Corradi, R. L. M. & Schwarz, H. E. 1993, *A&A*, 268, 714
 Di Stefano, R. 2010, *ApJ*, 719, 474
 Dilday, B., Howell, D. A., Cenko, S. B., et al. 2012, *Science*, 337, 942
 Eze, R. N. C., Luna, G. J. M., & Smith, R. K. 2010, *ApJ*, 709, 816
 Farrell, S. A., Gosling, A. J., Webb, N. A., et al. 2010, *A&A*, 523, A50
 Fertig, D., Mukai, K., Nelson, T., & Cannizzo, J. K. 2011, *PASP*, 123, 1054
 Galloway, D. K. & Sokoloski, J. L. 2004, *ApJ*, 613, L61
 Greene, A. E. & Wing, R. F. 1971, *ApJ*, 163, 309
 Haakonsen, C. B. & Rutledge, R. E. 2009, *ApJS*, 184, 138
 Halpern, J. P. & Gotthelf, E. V. 2010, *The Astronomer's Telegram*, 2681, 1
 Herbig, G. H. 2009, *AJ*, 138, 1502
 Iben, Jr., I. 1982, *ApJ*, 259, 244
 Ikeda, Y. & Tamura, S. 2004, *PASJ*, 56, 353
 Ishida, M., Okada, S., Hayashi, T., et al. 2009, *PASJ*, 61, 77
 Jorissen, A., Van Eck, S., Dermine, T., Van Winckel, H., & Gorlova, N. 2012, *Baltic Astronomy*, 21, 39

- Kaplan, D. L., Levine, A. M., Chakrabarty, D., et al. 2007, *ApJ*, 661, 437
- Karovska, M., Carilli, C. L., Raymond, J. C., & Mattei, J. A. 2007, *ApJ*, 661, 1048
- Karovska, M., Schlegel, E., Hack, W., Raymond, J. C., & Wood, B. E. 2005, *ApJ*, 623, L137
- Kennea, J. A., Mukai, K., Sokoloski, J. L., et al. 2009, *ApJ*, 701, 1992
- Kenny, H. T. & Taylor, A. R. 2005, *ApJ*, 619, 527
- Kylafis, N. D. & Lamb, D. Q. 1982, *ApJS*, 48, 239
- Livio, M. & Warner, B. 1984, *The Observatory*, 104, 152
- Luna, G. J. M. & Costa, R. D. D. 2005, *A&A*, 435, 1087
- Luna, G. J. M. & Sokoloski, J. L. 2007, *ApJ*, 671, 741
- Luna, G. J. M., Sokoloski, J. L., & Costa, R. D. D. 2006, *Ap&SS*, 304, 283
- Luna, G. J. M., Sokoloski, J. L., & Mukai, K. 2008, in *Astronomical Society of the Pacific Conference Series*, Vol. 401, RS Ophiuchi (2006) and the Recurrent Nova Phenomenon, ed. A. Evans, M. F. Bode, T. J. O'Brien, & M. J. Darnley, 342
- Luna, G. J. M., Sokoloski, J. L., Mukai, K., & Nunez, N. 2012, *The Astronomer's Telegram*, 3960, 1
- Marcu, D. M., Fürst, F., Pottschmidt, K., et al. 2011, *ApJ*, 742, L11
- Masetti, N., Bassani, L., Bird, A. J., & Bazzano, A. 2005, *The Astronomer's Telegram*, 528, 1
- Masetti, N., Dal Fiume, D., Cusumano, G., et al. 2002, *A&A*, 382, 104
- Masetti, N., Landi, R., Pretorius, M. L., et al. 2007, *A&A*, 470, 331
- Masetti, N., Munari, U., Henden, A. A., et al. 2011, *A&A*, 534, A89
- Masetti, N., Orlandini, M., Palazzi, E., Amati, L., & Frontera, F. 2006, *A&A*, 453, 295
- Masetti, N., Parisi, P., Jiménez-Bailón, E., et al. 2012, *A&A*, 538, A123
- McCullum, B., Bruhweiler, F. C., Wahlgren, G. M., Eriksson, M., & Verner, E. 2008, *ApJ*, 682, 1087
- Mikolajewska, J. 2007, *Baltic Astronomy*, 16, 1
- Montez, Jr., R., Kastner, J. H., & Sahai, R. 2006, in *Bulletin of the American Astronomical Society*, Vol. 38, American Astronomical Society Meeting Abstracts, 1029
- Muerset, U., Nussbaumer, H., Schmid, H. M., & Vogel, M. 1991, *A&A*, 248, 458
- Muerset, U., Wolff, B., & Jordan, S. 1997, *A&A*, 319, 201
- Mukai, K., Ishida, M., Kilbourne, C., et al. 2007, *PASJ*, 59, 177
- Munari, U. & Patat, F. 1993, *A&A*, 277, 195
- Munari, U. & Renzini, A. 1992, *ApJ*, 397, L87
- Narayan, R. & Popham, R. 1993, *Nature*, 362, 820
- Nelson, T., Mukai, K., Orio, M., Luna, G. J. M., & Sokoloski, J. L. 2011, *ApJ*, 737, 7
- Nichols, J. S., DePasquale, J., Kellogg, E., et al. 2007, *ApJ*, 660, 651
- Nomoto, K., Saio, H., Kato, M., & Hachisu, I. 2007, *ApJ*, 663, 1269
- Nucita, A. A., Carpano, S., & Guainazzi, M. 2007, *A&A*, 474, L1
- Nussbaumer, H., Schmid, H. M., Vogel, M., & Schild, H. 1988, *A&A*, 198, 179
- Orio, M., Zezas, A., Munari, U., Siviero, A., & Tepedelenlioglu, E. 2007, *ApJ*, 661, 1105
- Patat, F., Chandra, P., Chevalier, R., et al. 2007, *Science*, 317, 924
- Patel, S. K., Zurita, J., Del Santo, M., et al. 2007, *ApJ*, 657, 994
- Pereira, C. B., Landaberry, S. J. C., & da Conceição, F. 1998, *AJ*, 116, 1971
- Podsiadlowski, P. & Mohamed, S. 2007, *Baltic Astronomy*, 16, 26
- Poole, T. S., Breeveld, A. A., Page, M. J., et al. 2008, *MNRAS*, 383, 627
- Popham, R. & Narayan, R. 1995, *ApJ*, 442, 337
- Sanford, R. F. 1949, *PASP*, 61, 261
- Sanford, R. F. 1950, *ApJ*, 111, 270
- Santander-García, M., Corradi, R. L. M., Whitelock, P. A., et al. 2007, *A&A*, 465, 481
- Schmid, H. M. 1994, *A&A*, 284, 156
- Schmid, H. M. & Nussbaumer, H. 1993, *A&A*, 268, 159
- Seal, P. 1988, *The Symbiotic Star UV Aurigae*, ed. J. Mikolajewska, M. Friedjung, S. J. Kenyon, & R. Viotti, 293
- Smith, R. K., Mushotzky, R., Mukai, K., et al. 2008, *PASJ*, 60, 43
- Sokoloski, J. L. 2003, in *Astronomical Society of the Pacific Conference Series*, Vol. 303, Symbiotic Stars Probing Stellar Evolution, ed. R. L. M. Corradi, J. Mikolajewska, & T. J. Mahoney, 202
- Sokoloski, J. L. & Bildsten, L. 2010, *ApJ*, 723, 1188
- Sokoloski, J. L., Kenyon, S. J., Espey, B. R., et al. 2006a, *ApJ*, 636, 1002
- Sokoloski, J. L., Luna, G. J. M., Mukai, K., & Kenyon, S. J. 2006b, *Nature*, 442, 276
- Stute, M., Luna, G. J. M., & Sokoloski, J. L. 2011, *ApJ*, 731, 12
- Stute, M. & Sahai, R. 2009, *A&A*, 498, 209
- Thompson, T. W. J., Tomsick, J. A., Rothschild, R. E., in't Zand, J. J. M., & Walter, R. 2006, *ApJ*, 649, 373
- Tueller, J., Gehrels, N., Mushotzky, R. F., et al. 2005, *The Astronomer's Telegram*, 591, 1
- Van Eck, S. & Jorissen, A. 1999, *A&A*, 345, 127
- Van Eck, S. & Jorissen, A. 2002, *A&A*, 396, 599
- Wang, B. & Han, Z.-W. 2010, *Research in Astronomy and Astrophysics*, 10, 235
- Warner, B. 1995, *Cambridge Astrophysics Series*, 28
- Wheatley, P. J. & Kallman, T. R. 2006, *MNRAS*, 372, 1602

Table 4. X-ray spectral classifications of symbiotic stars.

	Object	Type	Reference
27	StH α 32	α	1, this work
	SMC 3	α	2
	Ln 358	α	2
	AG Dra	α	2
	Draco C-1	α	2
	RR Tel	α	2
	CD-43 14304	α	2
36	Y Cra ^a	β	this work
41	SWIFT J171951.7-300206	β	this work
	RX Pup	β	2, 3
	Z And	β	2, 4
	V1329 Cyg	β	5
	Mira AB	β	6
	EG And	β	2
	HM Sge	β	2
	V1016 Cyg	β	2
	PU Vul	β	2
	AG Peg	β	2
	Hen 2-104	β	24
1	NQ Gem	β/δ	this work
2	UV Aur	β/δ	this work
5	ZZ CMi	β/δ	this work
29	BI Cru ^b	β/δ	this work
32	V347 Nor	β/δ	this work
	R Aqr	β/δ	2, 7
	CH Cyg	β/δ	2, 8
	MWC 560	β/δ	23
6	ER Del	δ	this work
10	Hen 3-461	δ	this work
13	CD -283719	δ	this work
	RT Cru	δ	9, 10
	T CrB	δ	11
	SS73 17	δ	12, 13
	GX 1+4	γ	2
	Hen 3-1591 ^c	γ	2
	V934 Her	γ	14
	4U 1954+31	γ	15
	Sct X-1	γ	16
	IGR J16194-2810	γ	17
	IRXS J180431.1-273932	γ	18
	IGR J16358-4724	γ	19
	IGR J16393-4643	γ	20
	2XMM J174016.0-290337 ^d	γ	21
	CGCS 5926	γ	22

References. (1) Orio et al. (2007); (2) Muerset et al. (1997); (3) Luna et al. (2006); (4) Sokoloski et al. (2006a); (5) Stute et al. (2011); (6) Sokoloski & Bildsten (2010); (7) Nichols et al. (2007); (8) Mukai et al. (2007); (9) Luna & Sokoloski (2007); (10) Kennea et al. (2009); (11) Luna et al. (2008); (12) Eze et al. (2010); (13) Smith et al. (2008); (14) Masetti et al. (2002); (15) Masetti et al. (2006); (16) Kaplan et al. (2007); (17) Masetti et al. (2007); (18) Nucita et al. (2007); (19) Patel et al. (2007); (20) Thompson et al. (2006); (21) Farrell et al. (2010); (22) Masetti et al. (2011). (23) Stute & Sahai (2009); (24) Montez et al. (2006)

^(a) Although two components are needed to fit the X-ray spectrum, the emission extends only up to ~ 5 keV, with a small flux contribution above the ROSAT bandpass. ^(b) Questionable classification due to short exposure time. The presence of a soft β component needs confirmation. ^(c) Questionable classification. Hen 3-1591 has been observed only with ROSAT, therefore no information is available about its hard X-ray emission and the nature of the accreting object is not firm enough to secure its classification. The nature of the accreting object cannot be confirmed with the available ROSAT data. ^(d) Questionable classification. 2XMM J174016.0-290337 has also been classified as an IP after a period of 623 ± 2 s was found in the optical and X-rays (Halpern & Gotthelf 2010) but its X-ray spectrum is not that of a standard IP (Farrell et al. 2010).

Table 3. UVOT Timing analysis results. For those objects observed in more than one visit, we list the standard deviations, s and s_{exp} for each visit that contains more than two exposures. The mean count rate during each visit is listed under the column $\langle count\ rate \rangle$, while the s_{frac} represents the fractional rms variability amplitudes that we define as $s / \langle count\ rate \rangle$ or $s_{exp} / \langle count\ rate \rangle$ in the case of its upper limit.

	Object (UV Filter)	s [counts/s]	s_{exp} [counts/s]	s/s_{exp}	$\langle count\ rate \rangle$	s_{frac}
1	NQ Gem (UVM2)	31.2	1.1	28.4	204±8	0.15
4	TX CVn (UVW2)	4.0	1.0	4.0	241±2	0.02
	TX CVn (UVW2)	47.7	1.0	47.7	207±24	0.23
	TX CVn (UVM2)	37.0	1.0	37.0	152±21	0.24
5	ZZ CMi (UVM2)	1.0	0.3	3.3	24.8±0.3	0.04
	ZZ CMi (UVM2)	3.0	0.3	10.0	32.1±1.1	0.10
6	AR Pav (UVM2)	0.4	0.3	1.3	38.5±0.2	0.01
	AR Pav (UVM2)	0.7	0.2	3.5	36.3±0.3	0.02
7	ER Del (UVW2)	3.9	0.1	39.0	20.1±1.2	0.19
8	CD -27 8661 (UVM2)	1.5	0.2	7.5	17.7±0.5	0.08
9	V627 Cas (UVW2)	0.05	0.03	1.7	0.43±0.03	0.11
	V627 Cas (UVW2)	0.02	0.03	0.67	0.42±0.01	< 0.06
10	Hen 3-461 (UVM2)	0.64	0.06	10.7	3.8±0.2	0.17
11	Wray 16-51 (UVM2)	0.03	0.03	1.0	0.38±0.02	0.09
	Wray 16-51 (UVM2)	0.05	0.03	1.67	0.65±0.02	0.08
	Wray 16-51 (UVM2)	0.11	0.04	2.75	0.65±0.06	0.17
12	SY Mus (UVW2)	4.7	0.4	11.7	74.1±1.6	0.06
13	CD -28 3719 (UVW2)	5.4	0.2	27.0	37.5±1.7	0.14
14	V443 Her (UVM2)	5.2	0.4	13.2	85.4±3.0	0.06
	V443 Her (UVM2)	11.4	0.4	28.5	80.8±5.1	0.14
15	BD -21 3873 (UVM2)	0.4	0.4	1.0	59.8±0.3	0.01
	BD -21 3873 (UVM2)	1.0	0.1	10.0	5.8±0.4	0.17
18	V748 Cen (UVM2)	0.4	0.2	2.0	26.7±0.2	0.01
	V748 Cen (UVM2)	9.3	0.6	15.5	141±3	0.06
19	UKS Ce-1 (UVM2)	0.03	0.03	1.0	0.14±0.01	0.23
	UKS Ce-1 (UVM2)	0.01	0.02	0.6	0.16±0.01	< 0.14
20	YY Her (UVM2)	0.4	0.1	4.0	7.8±0.2	0.05
22	CI Cyg (UVM2)	0.4	0.3	1.3	41.4±0.2	0.01
	CI Cyg (UVM2)	0.18	0.19	0.97	37.4±0.1	< 0.01
	CI Cyg (UVM2)	1.2	0.2	6.0	36.7±0.5	0.03
23	FG Ser (UVM2)	0.01	0.02	0.5	0.36±0.01	< 0.06
	FG Ser (UVM2)	0.04	0.03	1.3	0.37±0.01	0.11
24	Wray 15-1470 (UVM2)	0.18	0.12	1.5	7.5±0.1	0.02
	Wray 15-1470 (UVM2)	0.11	0.20	0.6	7.6±0.1	< 0.01
	Wray 15-1470 (UVM2)	0.19	0.10	1.9	7.3±0.1	0.03
	Wray 15-1470 (UVM2)	0.81	0.14	5.8	6.9±0.5	0.12
25	Hen 3-863 (UVW2)	0.03	0.13	0.23	9.83±0.01	< 0.01
	Hen 3-863 (UVW2)	0.19	0.18	1.05	18.8±0.1	0.01
	Hen 3-863 (UVW2)	0.08	0.15	0.5	9.8±0.1	< 0.01
26	AS 210 (UVM2)	0.5	0.1	5.0	10.2±0.2	0.05
27	StH α 32 (UVM2)	0.1	0.1	1	11.1±0.1	< 0.01
	StH α 32 (UUU)	0.3	0.2	1.5	26.9±0.1	0.01
28	V835 Cen (UVW2)	0.06	0.08	0.7	2.9±0.1	< 0.02
	V835 Cen (UVM2)	0.03	0.03	1.0	0.82±0.01	< 0.04
29	BI Cru (UVW2)	0.07	0.09	0.8	5.0±0.1	< 0.02
	BI Cru (UVW2)	0.10	0.10	1.0	5.0±0.1	< 0.02
	BI Cru (UVW2)	0.01	0.08	0.12	5.1±0.1	< 0.02
	BI Cru (UVW2)	0.07	0.13	0.54	5.3±0.1	< 0.02
30	AS 289 (UVM2)	0.04	0.03	1.3	0.46±0.01	0.08
	AS 289 (UVM2)	0.01	0.04	0.25	0.49±0.01	< 0.08
32	V347 Nor (UVW2)	0.01	0.02	0.5	0.12±0.01	< 0.22
	V347 Nor (UVW2)	0.02	0.02	1.0	0.11±0.01	< 0.23
	V347 Nor (UVM2)	0.01	0.03	0.30	0.11±0.01	< 0.24
	V347 Nor (UVM2)	0.01	0.01	1.0	0.04±0.01	< 0.26
33	AX Per (UVW2)	1.13	0.54	2.09	108.7±0.3	0.01
34	Hen 3-1213 (UVM2)	0.08	0.08	1.0	3.03±0.03	0.03
35	LT Del (UVM2)	0.33	0.15	2.2	10.7±0.1	0.03
36	Y Cra (UVM2)	0.28	0.12	2.3	15.7±0.1	0.02
37	AS 327 (UVM2)	0.08	0.08	1.0	2.39±0.05	0.03
	AS 327 (UVM2)	0.07	0.07	1.0	2.42±0.03	0.03
	AS 327 (UVM2)	0.04	0.06	0.7	2.44±0.01	< 0.02
39	KX Tra (UVM2)	2.4	0.5	4.8	59±1	0.04
	KX Tra (UVM2)	3.8	0.2	16	57±1	0.07
40	V366 Car (UVM2)	0.06	0.07	0.8	4.03±0.02	< 0.02
41	SWIFT J171951.7-300206 (UUU)	2.05±0.14	...

Table 3. continued.

Object (UV Filter)	s [counts/s]	s_{exp} [counts/s]	s/s_{exp}	$\langle count\ rate \rangle$	s_{frac}
SWIFT J171951.7-300206 (UVM2)	<0.04	...
SWIFT J171951.7-300206 (UVW1)	0.37 ± 0.03	...
SWIFT J171951.7-300206 (UVW2)	0.17 ± 0.02	...